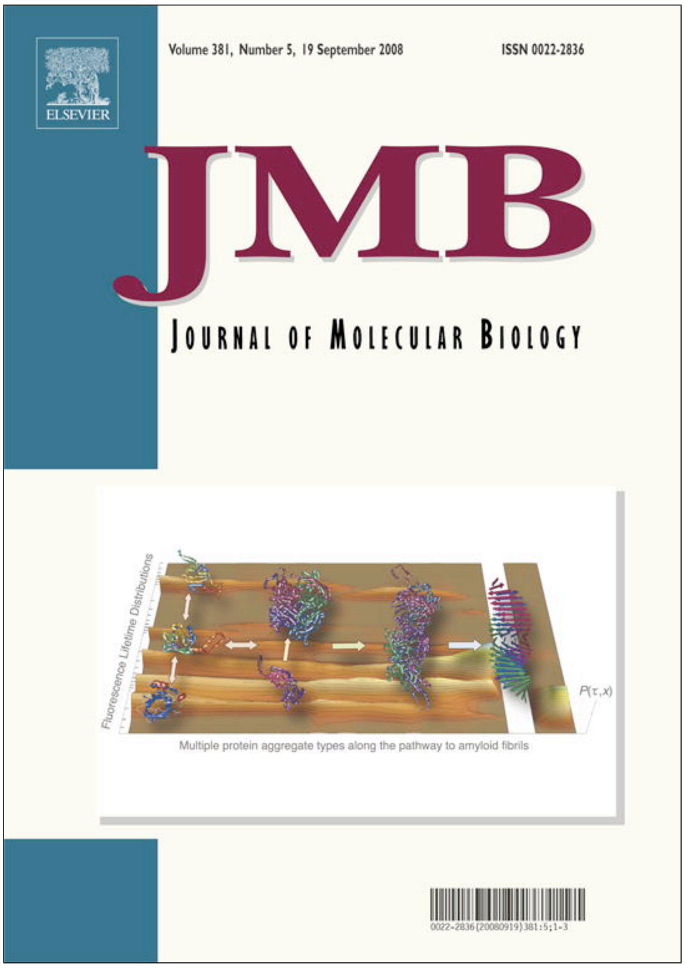
Volume 381, Number 5, 19 September 2008
ISSN 0022-2836
ELSEVIER
JMB
Journal of Molecular Biology
Fluorescence Lifetime Distributions
P(τ,x)
Multiple protein aggregate types along the pathway to amyloid fibrils

doi:10.1016/j.jmb.2008.06.043 J. Mol. Biol. (2008) 381, 1332–1348

JMB Available online at www.sciencedirect.com ScienceDirect ELSEVIER

β-Lactoglobulin Assembles into Amyloid through Sequential Aggregated Intermediates

Jason T. Giurleo, Xianglan He and David S. Talaga*

Department of Chemistry and Chemical Biology, Rutgers, The State University of New Jersey, 610 Taylor Road, Piscataway, NJ 08854, USA

Received 8 April 2008; received in revised form 22 May 2008; accepted 16 June 2008
Available online 20 June 2008

Edited by K. Kuwajima

We have investigated the aggregation and amyloid fibril formation of bovine β-lactoglobulin variant A, with a focus on the early stages of aggregation. We used noncovalent labeling with thioflavin T and 1-anilino-8-naphthalenesulfonate to follow the conformational changes occurring in β-lactoglobulin during aggregation using time resolved luminescence. 1-Anilino-8-naphthalenesulfonate monitored the involvement of the hydrophobic core/calyx of β-lactoglobulin in the aggregation process. Thioflavin T luminescence monitored the formation of amyloid. The luminescence lifetime distributions of both probes showed changes that could be attributed to conformational changes occurring during and following aggregation. To correlate the luminescence measurements with the degree of aggregation and the morphology of the aggregates, we also measured dynamic light scattering and atomic force microscopy images. We evaluated the relative stability of the intermediates with an assay that is sensitive to aggregation reversibility. Our results suggest that initial aggregation during the first 5 days occurred with partial disruption of the characteristic calyx in β-lactoglobulin. As the globular aggregates grew from days 5 to 16, the calyx was completely disrupted and the globular aggregates became more stable. After this second phase of aggregation, conversion into a fibrillar form occurred, marking the growth phase, and still more changes in the luminescence signals were observed. Based on these observations, we propose a three-step process by which monomer is converted first into weakly associated aggregates, which rearrange into stable aggregates, which eventually convert into protofibrils that elongate in the growth phase.

Keywords: lipocalin; fluorescence; dynamic light scattering; protein aggregation; amyloid

Introduction

Amyloid formation

Aggregation of soluble polypeptides or proteins into insoluble amyloid fibrils containing the cross-β structural motif has been observed in the progression of more than 20 diseases.[1] The human health impact of these diseases has motivated intensive study and numerous reviews of the structure and growth of amyloid fibrils.[1–9]

Amyloid formation often shows a sigmoidal kinetic growth pattern. Early times are characterized by a lag phase, where little or no fibrillar growth is observed. The growth phase, where amyloid rapidly assembles, follows. The reaction then slows, with amyloid accumulation reaching a plateau.[1,10,11] After this point, amyloid often begins to gel or precipitate *in vitro*. The durations of the lag phase and the growth phase both change dramatically depending on the incubation conditions.[12–14]

The kinetic lag phase for many amyloidogenic precursors is characterized by conversion of soluble monomers into small oligomers.[10,14,15] One of the

*Corresponding author. E-mail address: talaga@rutgers.edu.

Abbreviations used: AFM, atomic force microscopy; ANS, 1-anilino-8-naphthalenesulfonate; β-LGa, β-lactoglobulin variant A; GIPG, globally regularized interior point gradient; DLS, dynamic light scattering; ThT, thioflavin T; AggA, aggregate A; AggB, aggregate B; APTES, aminopropyltriethoxysilane; TCSPC, time-correlated single-photon counting.

driving forces for initial aggregation of soluble globular proteins may be the partitioning of hydrophobic side chains into a central core, much like protein folding.[16] The structural content and contribution to amyloid assembly of the small oligomers are usually only inferred.[17,18] During the lag phase, there is little appreciable amyloid formation, as determined by histological assays. The lag time can be reduced or eliminated by addition of mature amyloid, as observed *in vivo* by mortality of the organism and/or autopsy with histological staining[19] and as observed *in vitro* by light scattering or staining.[12,20,21] This leads most investigators to associate the lag phase with the formation of a critical seed or nucleus.[15,17,20,22] The kinetic evidence of a critical seed has not been corroborated by either structural evidence identifying it or direct mechanistic information on how it forms and grows.

The kinetic growth phase shows rapid assembly of amyloid. Amyloid filaments and fibrils have been identified in atomic force microscopy (AFM) and electron microscopy images during and after the growth phase.[21,23–26] During the growth phase, it is most often observed that the kinetic rate is first order with respect to precursor concentration.[13,27,28] Based on images and simple kinetics, mechanisms have been proposed,[11] but are not well-established. A template or seed has been proposed to be required for the growth phase to occur.[29] Growth then occurs as the template either actively induces structural changes in other species or passively aggregates with other species with the correct template.[30] Recent evidence has shifted some of the focus from amyloid fibrils to prefibrillar amyloidogenic aggregates as the cause of Alzheimer's disease symptoms,[2,18] leading many to propose the development of vaccines targeting small amyloidogenic aggregates.[4,6,31] Distinguishing between small oligomers that are harmless and those that either are toxic in their own right or lead to formation of amyloid fibrils remains a challenge.[18]

Many amyloidogenic peptides and proteins exhibit conformational polymorphism; they can exist in multiple stable conformations.[32] Conformational changes are typically observed during amyloid assembly. In their native state, the precursor proteins may not, in general, contain the secondary structural elements present in the final amyloid assembly.[33] The amide I infrared absorption or Raman band has been observed to lose intensity associated with the native state and to gain intensity associated with cross-β.[25,32,34,35] Circular dichroism of the peptide backbone absorption band is also sensitive to secondary structure and has given similar results.[36,37] Fluorescence spectroscopy has been used to detect conformational changes either by noncovalent labeling with dyes such as 1-anilino-8-naphthalenesulfonate (ANS) that are specific for exposed hydrophobic patches[38–41] or by covalent attachment of fluorescent dyes.[42,43]

Bovine β-lactoglobulin variant A

We investigate the mechanism of amyloid formation from β-lactoglobulin variant A (β-LGa), with a particular focus on the aggregation and structural changes occurring during the lag phase. Bovine β-LGa (molecular mass, 18.3 kDa/monomer) is a member of the lipocalin superfamily of proteins consisting of a flattened β-barrel or calyx comprising eight β-strands (Fig. 1). β-LGa also has a partial ninth β-strand and a three-turn α-helix.[45] β-LGa is dimeric under native conditions. β-LGa has two disulfide bridges and a single free cysteine that has been observed to undergo disulfide exchange only when denatured.[46]

β-LGa has been shown to form amyloid fibrils.[13,25,37,47] The folding behavior of β-LGa has been extensively studied using bulk experiments.[46] β-LGa has structural elements that are conformationally labile.[48–53] β-LGa can exist in an equilibrium between folded, partially structured, and unfolded states.[13,37,48–58] β-LGa has been reported to form nonnative α-helices prior to complete folding.[13,49–56] NMR has shown that these α-helices must melt and form a β-strand to complete the native-state

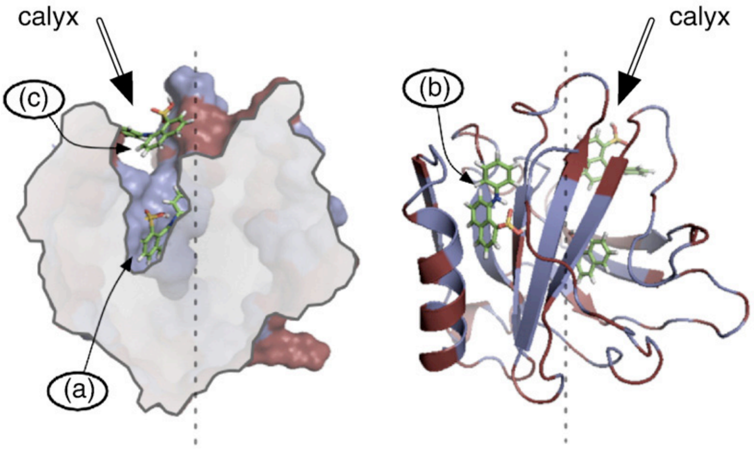

Fig. 1. The possible binding sites of ANS to β-LGa. Hydrophobic amino acid residues are in slate; hydrophilic residues are in brick. ANS was docked to β-LGa using PyMOL and minimized using the molecular mechanics software IMPACT.[44] The left panel is a 16-Å slab of the van der Waals surface without secondary structure illustrating the binding of ANS in the hydrophobic calyx site (a). The right panel is rotated 90° about the vertical axis of the left panel to show the postulated intercalation site in the hydrophobic region between the main α-helix and the β-barrel surface patch (b). Roughly two-thirds of the calyx volume is represented by its "mouth" and may be considered to be a third ANS binding site (c).

structure.[53] The stabilization of β-LGa by trehalose was studied using acrylodan covalently attached to cysteine 121, which showed conformationally sensitive fluorescence. Conformational fluctuations in β-LGa were transmitted to the local environment of the attached acrylodan, resulting in a spectral shift, as well as in lifetime, intensity, and anisotropy changes.[59]

Biophysical approaches to aggregation

In this study, we use ANS fluorescence lifetime distributions to follow the aggregation of β-LGa through its lag-phase intermediates until it forms amyloid fibrils. It has been previously reported that the fluorescence lifetime of ANS is influenced by the polarity of its binding environment, specific interactions with amino acid side chains, and the relative orientation and mobility of the anilino group.[60] ANS binds to hydrophobic regions of proteins[61] and has been extensively used to probe the presence of the molten globule state and the assembly of partially structured proteins.[13,40,62] ANS has been observed to have different fluorescence intensity properties when bound to different types of protein aggregates.[63] β-LGa binds ANS in several ways[59]; one way is through the calyx, which results in a sequestered ANS with a very long lifetime (see Fig. 1). ANS probes both the presence and the integrity of this calyx as well as the overall exposure of hydrophobic groups in β-LGa. The calyx is of particular interest because it is the majority of the hydrophobic core of β-LGa. Disruption of this core is required for an aggregate to fulfill the geometric constraints of the cross-β structure of an amyloid fibril. We use our globally regularized interior point gradient (GIPG) fitting procedure that fits all the data simultaneously to resolve the contributions of different ANS binding sites to the fluorescence lifetime decay.[64]

We expect aggregation to be driven, in part, by hydrophobic forces. Therefore, the parts of the protein that can bind ANS should be structurally changed by aggregation. The ability to detect the presence of an intact calyx by virtue of ANS binding allows determination of the involvement of, and structural changes in, the protein hydrophobic core during amyloidogenic incubation. If the aggregation process is hydrophobically driven, then we expect the aggregate to sequester hydrophobic residues changing the structure of the calyx. Alternatively, if hydrophobicity is the key driving force for conversion into the cross-β structure, then the large changes in the calyx should occur at that point in the incubation. In either case, the sensitivity of ANS to its binding environment should be reflected in its fluorescence lifetime distribution.

We confirm early stages of aggregation using dynamic light scattering (DLS). DLS has been used extensively to characterize protein aggregation and the growth of amyloid.[65,66] We explicitly evaluate the evolution of the particle size distribution using the GIPG fitting procedure.[64]

We assay for the presence of amyloid using thioflavin T (ThT) luminescence. When bound to amyloid, ThT exhibits a new absorption band at 450 nm, which has been attributed to ThT binding to the cross-β structure.[13,67–70] The spectroscopic properties of ThT in amyloid are consistent with a behavior that has been attributed to ThT dimer formation.[71–73] The lifetime of such a dimer will depend on its environment and geometry, and some contribution of the luminescence may arise from non-amyloid-binding modes.[74] Using a ThT luminescence lifetime assay, we exploit this to detect the presence of various amyloid-like structures. The different lifetime distribution contributions and their evolution are determined using the GIPG procedure.

We determine the morphology of the aggregates using AFM imaging. Imaging techniques such as AFM have provided an invaluable way to determine the gross morphology of amyloid protofibrils (single-stranded) and fibrils (multistranded).[23,25,26,75]

Results

AFM shows sequential growth of aggregates

Figure 2 shows AFM images taken on several days of the incubation. The images are false-colored by height to emphasize the contrast between different classes of particles. AFM images taken from days 0 to 9 of the incubation did not show significant signs of aggregation. The protein deposited as a uniform coating on the functionalized mica surface (brown background in Fig. 2). Starting from day 10 of the incubation, we began to see small round aggregates (green dots in Fig. 2) that grew in size and number through day 22 (orange dots in Fig. 2). After day 22, the number and length of oblong protofibrils increased (purple bars in Fig. 2). Eventually, long fibrillar aggregates were observed (Fig. 2). Large amorphous aggregates were also observed (white features in Fig. 2) but appeared to evolve independently of the other species.

The AFM results suggest two acts to aggregate growth. The first act consists of formation of round aggregates that can be stably imaged on the functionalized mica surface. The second act features the elongation of protofibrils. Each of these processes appears to have an induction period of 8–10 days under our incubation conditions. A complete analysis of the evolution of the AFM particle size distribution is the subject of a forthcoming article.

DLS resolves early lag-phase aggregation

DLS correlation functions were measured every 15 min for 4.7 days to investigate the earliest aggregation events. Distributions of correlation decay times appear in Fig. 3. The width at 5 M urea was greater than it was at both lower and

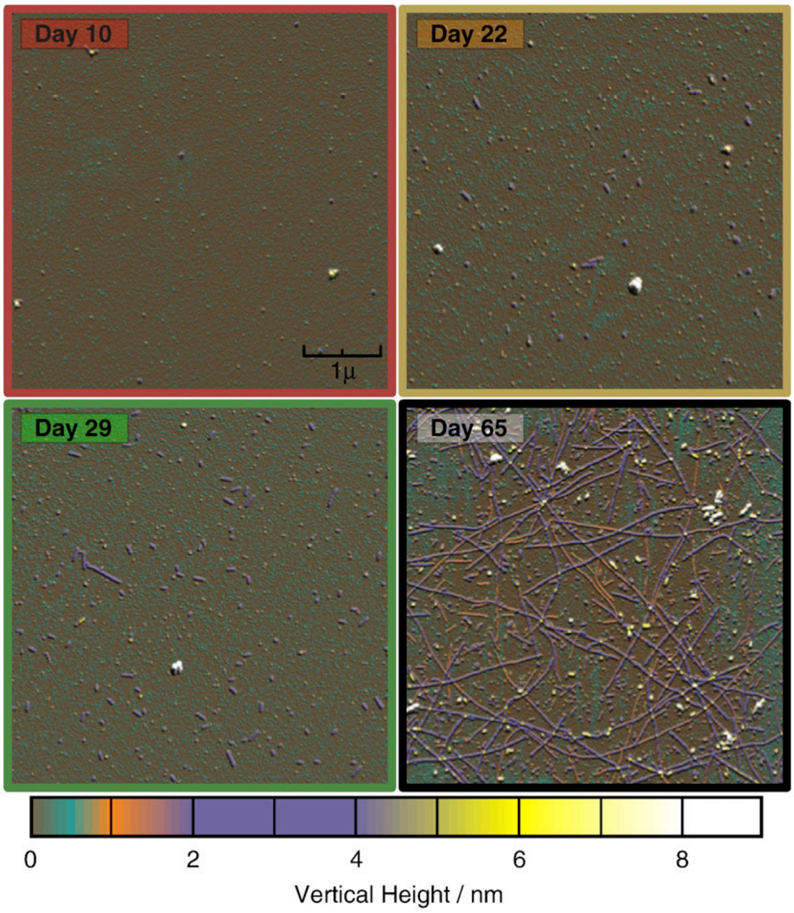

Fig. 2. AFM images of β-LGa aggregation under amyloidogenic conditions. Days 10, 22, 29, and 65 are shown as labeled. Images are colored by height and approximately correspond to species described in the text. AFM heights are uncorrected for tip penetration of the soft samples. Prior to day 10, there was little indication of stable aggregates adhering to aminosilanized mica surface. The first sign of small stable oligomers (in green) appears on day 10. The total number and aspect ratio of the aggregates increase through day 22. After 4 weeks, small protofibrillar species are apparent and range from 50 nm to several hundred nanometers in length. Fibrillar species ranging in height and length dominate at 2 months of incubation. Large amorphous aggregates appear as early as day 10, but appear to be off the amyloid formation pathway.

higher urea concentrations, where the protein is a native monomer (2.5 M) and is unfolded (7.5 M), respectively. This was consistent with literature reports that at 5 M at neutral pH, β-LGa intermediate and denatured states are in thermal equilibrium.[76] From days 0 to 2, the position of the peak maximum moved from the monomer decay time to the dimer decay time. By day 4 of incubation, the peak maximum has moved to the position expected for the tetramer decay time.

Figure 4 shows the evolution of the DLS decay time distribution taken every 2 days for the first 28 days of incubation. The 0- to 4-day evolution matches that of Fig. 4. The peak maximum of the small aggregate region did not substantially change after day 4. The peak width was broader than expected for a monodisperse tetrameric aggregate. From days 10 to 18, a shoulder appears (Fig. 4) to lengthen decay times, suggesting the growth of a minority species of larger aggregates. A weak and

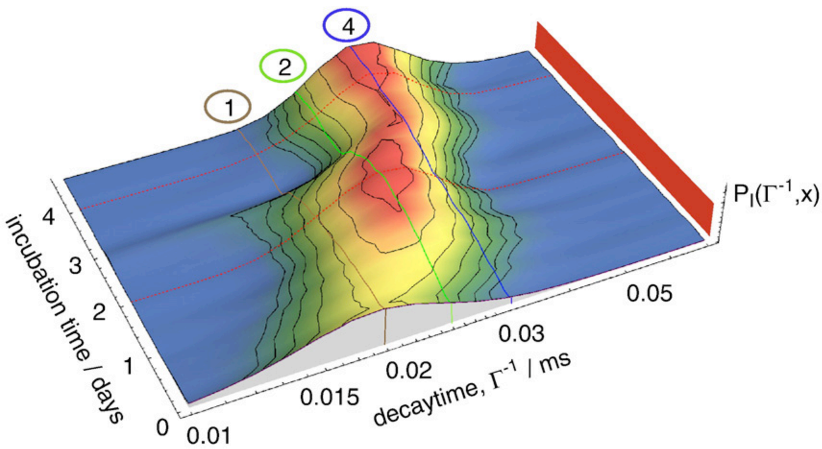

Fig. 3. GIPG fit of DLS correlation functions for the 4.7-day incubation of β-LGa. A continuous-acquisition DLS experiment allowed investigation of the earliest aggregation events. During the first hour of incubation, the hydrodynamic radius of β-LGa was consistent with a partially unfolded monomer at 2.5 nm [shown as a brown mesh line (1)]. If the aggregation preserves the density, the decay times of approximately spherical dimeric and tetrameric species can be calculated; they are represented by the green (2) and blue (4) mesh lines, respectively. The monomer was converted to mostly dimer by day 2, then to tetramer by day 4.

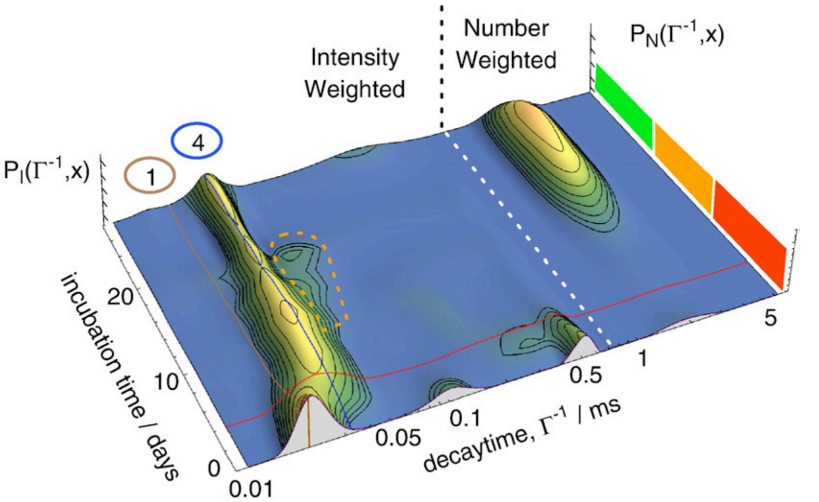

Fig. 4. GIPG fit of DLS correlation functions for the 28-day incubation of β-LGa. Mesh lines (1) and (4) are the same as in Fig. 3. The high-resolution DLS fits coincide with the first few days of the 28-day incubation. A shoulder appeared on day 10 and separated from the tetramer species on day 18 (orange dashed contour). This feature has a decay time characteristic of a small inflexible rod with length ranging from 15 to 30 nm, with the same radius as the tetramer. The red, orange, and green bars represent a rough estimate of the early, middle, and late phases that we have consistently observed throughout our experiments. The white mesh line demarcates the intensity and number-weighted representation of the decay times, allowing the entire data set to be presented together.

broad peak grows slowly from days 12 to 18 at ~1.5 ms and becomes appreciable from days 18 to 28. At these later stages, the large distribution of particle sizes and shapes prevents specification of these quantities in terms of the ensemble-averaged DLS decay time distribution.

Interpretation

The DLS data suggest three phases of aggregation. Aggregation of the monomer proceeded rapidly within the first few days of incubation. Nonreducing SDS-PAGE analysis after 5 days of incubation showed mainly disulfide-linked dimers with some monomers. The motility of the monomers that were still present was consistent with their native disulfides still being intact. This suggests that oxidative aggregation does not exceed the dimeric state, consistent with only a single exchanging cysteine per monomer. Upon accumulation of the approximately tetrameric aggregate, a new phase begins. Further changes showing increases in particle size appeared during days 10–18, suggesting another mode of aggregation. The contribution of these particles to the DLS signal eventually was swamped by the contribution of the large particles that appeared in significant numbers from day 18 onward. Late-stage (>30 days of incubation) SDS-PAGE showed similar results, with the concentration of the dimers being about 50% that of the monomers. Again, the motility of the monomers was greater under the nonreducing conditions than under reducing conditions. The lack of disulfide cross-linked aggregates of higher order than dimers at late stages is consistent with higher-order aggregation being associated with non-covalent interactions.

ThT tracks structural conversions

We used a ThT assay to evaluate the point in the incubation when the aggregates converted into amyloid. Steady-state luminescence measured during incubation shows the classic sigmoid curve that is often associated with amyloid formation. As seen in Fig. 5, the individual lifetime contributions to the signal, however, have a very different behavior.

When measured in buffer, ThT shows four contributions to the lifetime distribution, and we speculate that the different lifetimes arise from different ThT aggregate geometries that are free in solution.[71] ThT in the presence of unincubated β-LGa shows an additional lifetime contribution at ~110 ps that is not present in the protein-free control. β-LGa is known to bind hydrophobic molecules; therefore, some luminescence changes associated with this binding to the monomer are expected. It is also possible that a single β-LGa could bind two ThT molecules, creating a small amount of dimer signal, as was shown by intercalation of ThT in γ-cyclodextrin.[72,73]

The ThT lifetime distribution was substantially different at each phase of the incubation. During the beginning of the lag phase (days 0–5), we saw a decrease in the contributions that are present in the ThT-only control. The relative contributions of these components also change. This behavior suggests that the aggregation in the early lag phase reduces the solution-phase portion of the ThT in favor of protein-partitioned ThT. During the lag phase (days 9–18), we saw a different pattern emerge in the lifetime distribution. Several new lifetime features ranging from 75 ps to 2.2 ns appeared.

After day 18, the distribution began to change rapidly, as shown by the growth of a feature at 2.6 ns, followed by a feature at 1.3 ns. On day 32, the majority of the luminescence signal came from the 580-ps lifetime. The short-lifetime feature at 11 ps disappeared and was replaced by a feature at 18 ps that attained a maximum at 26 days and then disappeared by 33 days. After 2 months of incubation, the distribution was dominated by a broad asymmetric peak at 2.6 ns, with a smaller contribution at 250 ps.

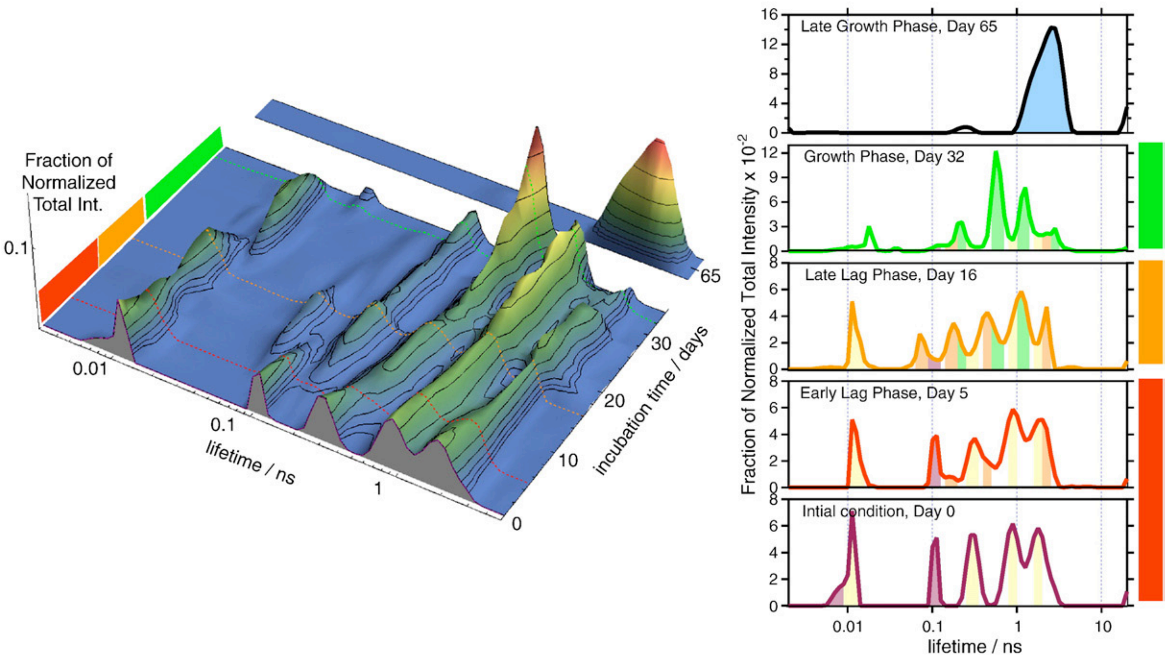

Fig. 5. GIPG fit of ThT luminescence decays in the presence of β-LGa over a 28-day incubation. Left panel: The evolution of lifetime distributions shows that the onset of luminescent species occurs in stages. The reduced chi-square (χ^2_r) value for this global fit was 1.022. Right panel: Incubation time slices of ThT lifetime distributions with different contributions on days 0, 5, 16, 32, and 65 are as labeled and correspond to the dotted mesh lines in the right panel. To depict the growth and loss of different luminescence components along the incubation time course, the distributions are filled to the baseline with colors corresponding to the trace where the particular component dominates. For example, the green filling matches the peaks on day 32, but the same components are less prevalent on day 16.

There are clearly multiple contributions to the ThT lifetime distribution. Each phase of the incubation has a distinct lifetime distribution, suggesting that ThT associates with many different aggregates in structurally different ways. We observed that significant ThT luminescence grew during the earliest stages of incubation (Fig. 5). These changes in an intensity-only experiment might be interpreted as a baseline shift. The association of monomers into a disordered aggregate may provide ThT the opportunity to form dimers that show luminescence similar to that of amyloid; however, the lack of regular geometry results in a different lifetime. Particularly striking is the difference between the 580-ps contribution that seems to appear in association with protofibrils and the 2.6-ns contribution that appears in the late-stage aggregation where mature amyloid fibrils are present. The signal from ThT that is usually associated with histological staining is probably most closely related to the distribution from the 65-day sample. The ThT signal changes that contribute to the classic sigmoidal intensity kinetic trace are most likely due to other binding modes and luminescence lifetimes. This suggests that the proamyloid ThT luminescence has a structural sensitivity that is reflected in its luminescence lifetime distribution. ThT assays based only upon intensity could be misleading, since there are several contributions to the luminescence that are potentially changing during incubation. The contributions from the different species cannot be resolved from intensity alone.

ANS reports changes in hydrophobic regions and calyx loss

The fluorescence lifetime of ANS was measured during 28 days of amyloidogenic incubation. We used GIPG as a model-free approach to determine the evolution of the ANS fluorescence assay lifetime distribution. We observed several peaks in the distribution that change systematically with incubation time and labeled them (a) though (i) for clarity, as shown in Fig. 6. Some of these peaks change during the first several days of the incubation. Others grow at the late stages of the incubation. The evolution of individual peaks can be associated with the changes in the availability of specific binding environments on β-LGa in its various aggregation states. To directly evaluate the evolution of the contributions from each subpopulation of ANS, we constructed a reduced-basis set representing each peak from the original GIPG fit as a separate function. The Laplace transform of each of these peaks was convoluted by the instrument response function in this simplified basis set. The population of each contribution as a function of incubation time appears in Fig. 7. These subpopulations of ANS binding were then assembled into lifetime

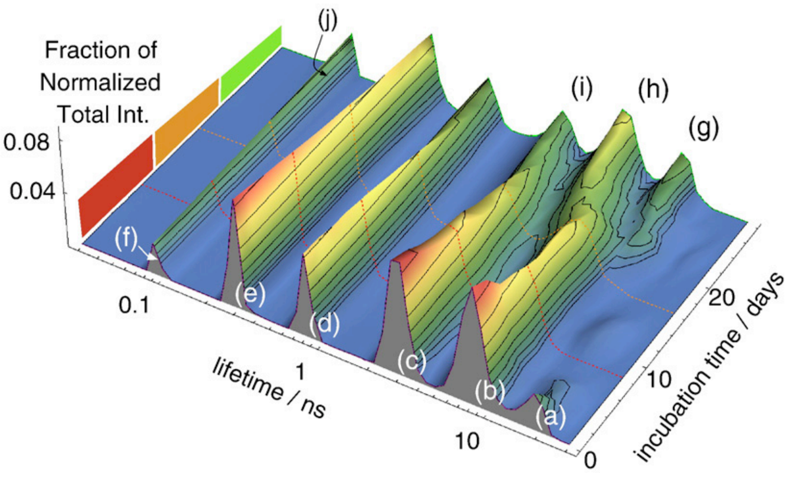

Fig. 6. GIPG fit of ANS fluorescence decays in the presence of β-LGa over a 28-day incubation. The χ^2_r for this global fit was 1.019. The distribution of fluorescence lifetimes showed the variety of binding environments for ANS and their systematic population changes with incubation time. The reduction of some peaks (i.e., a, b, and c) and the increase of others (i.e., g, h, and i) reflected the conformational changes experienced by β-LGa as it assembles into fibrils. All peaks are assigned to different ANS environments in the text. This model-free fit was used as the basis for further data reduction as described in the text and as shown in Fig. 7.

distribution fingerprints for the different species along the amyloid-formation pathway.

ANS is quenched by full exposure to 5 M urea and gave a lifetime of ~300 ps (e) in our control experiments. This contribution appeared to decrease as the incubation progressed. This suggested an increase in the partitioning of ANS with the protein as compared to the solution and was consistent with an overall increase in the availability of hydrophobic binding sites as the incubation proceeded.

The model-free GIPG fit in Fig. 6 shows an 89-ps feature (f), which was also present in the ANS lifetime distribution from 1 to 6 M urea in our control experiments, but only when β-LGa was also present. This feature appeared to increase in population from days 0 to 14, then to decrease from days 16 to 28. The 89-ps contribution overlapped with a broad lifetime contribution at 70 ps (j) that grew starting on day 18. The increase in this contribution appeared to compensate for the loss of the 89-ps contribution. These lifetimes were significantly shorter than that of the free ANS, suggesting a quenching interaction with an amino acid side chain.

The monomeric signal included contributions from peaks at 18.2 ns (a), 7.9 ns (b), and 2.7 ns (c). The peak at 18.2 ns was close to the unquenched lifetime of ~19 ns predicted by an evaluation of oscillator strength using the Strickler–Berg equation.[77] This suggested that ANS was sequestered from any quencher and was protected from water, consistent with an intact calyx. This feature decreased throughout the incubation. ANS can induce structure in proteins, and the presence of folded β-LGa under these conditions may be a result of this effect. No other lifetime feature in the distribution appears to compensate for the loss of the 18.2-ns feature.

The peak at 7.9 ns (b) also suggested protection from water, although to a lesser degree. This was consistent with a partially denatured calyx. The 7.9-ns feature decreased dramatically in the first 8 days, leveling off until day 18, whereupon it continued to decrease. The changes in the 7.9-ns contribution appeared to be mostly compensated for by changes in a feature at 4.9 ns (h). The highly anticorrelated behavior of the 7.9- and 4.9-ns components suggested that the 4.9-ns feature was from ANS bound to β-LGa that had its 7.9-ns calyx site disrupted by aggregation.

The peak at 2.7 ns (c) has been previously attributed to β-LGa surface binding.[76] Based on our ANS docking studies, we found that the mouth of the calyx is a more likely assignment for this feature. The 2.7-ns feature decreased rapidly at first, with its evolution slowing after 8 days and accelerating again during the late stages of incubation. The 2.7-ns feature population changes were partly compensated for by changes in the 2.1-ns feature (i). Again, this close relationship leads us to conclude that the mouth of the calyx is disrupted during the process that exchanges the population of the 2.7- and 2.1-ns features.

Overall, the changes in the ANS lifetime distributions occurring after day 20 were more dramatic. One of these was an 11-ns feature (g) that appeared to grow at the late stages of incubation. The long lifetime suggests that ANS was mostly isolated from water. We attribute it to sequestration of ANS in the cross-β structure of amyloid protofibrils.

Not all of the lifetime features changed over the incubation time course. The feature at 790 ps (d) was present throughout the incubation, with only small changes in intensity. Therefore, the 790-ps site should be a structure that was not disrupted in the aggregation process. This lifetime was consistent with surface binding, which should be present at all points of the incubation. The 790-ps lifetime appeared to shift slightly at different points in the fits presented in Fig. 6. These shifts were too small to reliably resolve multiple lifetime contributions to this feature.

Any particular ANS lifetime peak can, in principle, contribute to several different aggregates. As reflected in the lifetime, the binding location, but not the specific aggregation state, is sensitive to the local

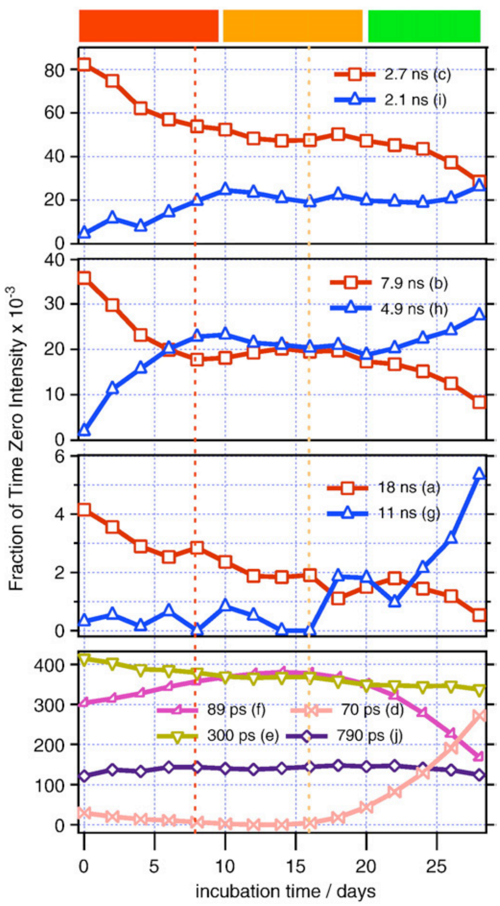

Fig. 7. Subpopulations of ANS binding to β-LGa over a 28-day incubation using GIPG with a reduced basis set. The χ^2_r for this global fit was 1.020. In the top three panels, the red squares represent decreasing lifetimes, and the blue triangles represent increasing lifetimes corresponding to the subpopulations in Fig. 6. The species lifetime evolutions are associated with a change in the ANS environment in the calyx or surface sites. The bottom panel shows the trends of the short lifetime components. (a) through (i) match the peaks in Fig. 6. The red and orange dotted vertical lines mark the lifetime components on days 8 and 16, which were combined with those on days 0 and 28 to generate the characteristic "fingerprints" of the ANS-bound protein species and are shown in Fig. 8.

environment. Nevertheless, the relative contribution of each binding site to a particular aggregate should be in some fixed proportion that depends on the structure of the β-LGa monomers in it. During amyloidogenic incubation, we see three main phases in the kinetic evolution of the ANS lifetime distribution that are corroborated by other experiments. We seek to separate the contributions of at least four species with qualitatively different aggregation states.

We assumed that the contributions of different species could be expressed as linear combinations of a multipeaked "fingerprint" describing both the relative binding likelihood and the nature of the various binding modes of ANS in each species. The first fingerprint describes the lifetime distribution of the various monomeric and monomer-like components. It was assigned from the day 0 β-LGa urea titration control experiments. The monomer fingerprint was subtracted from the day 8 reduced-basis GIPG lifetime distribution at a level that maintained nonnegativity of the distribution to obtain a difference fingerprint. We assumed that this difference fingerprint was due to an early oligomeric species that we designated "aggregate A" (AggA). The first two fingerprints were removed from the day 16 distribution to obtain a fingerprint that we designated "aggregate B" (AggB). The first three fingerprints were removed from the final distribution to obtain the fingerprint for "protofibrils." Fingerprints for the unbound ANS at 300 ps (e) and the surface ANS at 750 ps (d) were included separately into the fits. These fingerprints appear in Fig. 8. The rationale for the designations of the different fingerprints is in the Discussion.

Specific differences in the contributions of the different ANS lifetime peaks can be noted for the different fingerprints. The monomer fingerprint had a ratio [7.9 ns (b) and 2.9 ns (c)] different from that of AggA, which also lacks the 18-ns contribution (a). The contribution from the 89-ps peak (f) increased in the AggA fingerprint, which also had a new contribution at 4.9 ns (h). The AggB fingerprint is

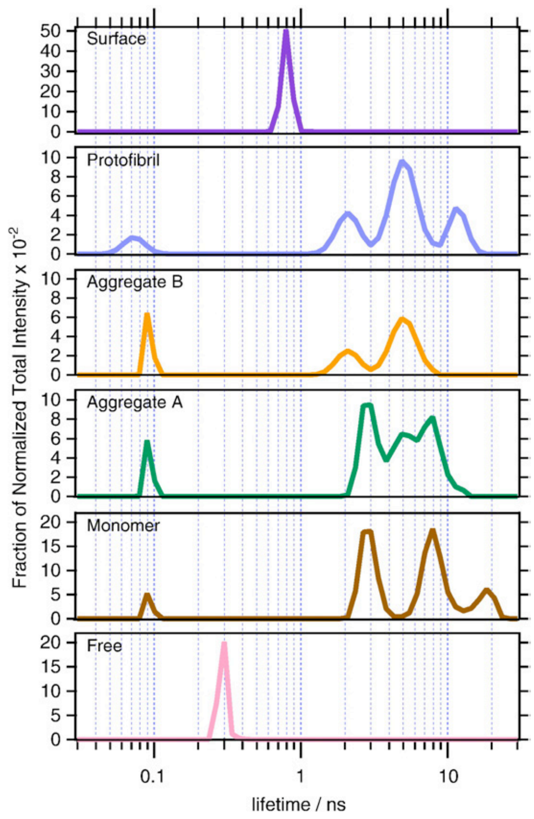

Fig. 8. The characteristic "fingerprint" lifetime distributions of ANS-bound β-LGa. The evolution of the ANS lifetime distributions was decomposed into "fingerprint" for each species. The fingerprints are labeled in the figure and used to fit the TCSPC decays with GIPG.

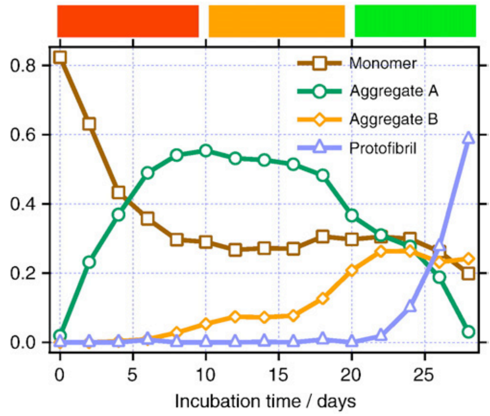

Fig. 9. The evolution of each fingerprint's contribution to the ANS β-LGa fluorescence decays. The χ^2_r for the global fit was 1.026. The evolution of the monomer, AggA, AggB, and protofibril showed multiple stages of aggregation. The monomeric species decreased dramatically in the first several days and is consistent with the DLS fits shown in Fig. 3. The increase in AggB from days 10 to 22 matched the accumulation of stable round aggregates in the AFM results. The increase in the number of protofibril species after day 24 coincided with significant changes in the ThT lifetime distributions and rodlike particles imaged by AFM.

missing the 7.9- and 4.9-ns components, and gained a new contribution at 2.1 ns (i). The protofibril fingerprint gains a peak at 11 ns (g) and trades the 89-ps contribution for the 70-ps feature (j). If a particular aggregation step does not result in a structural change, then it will not be reflected in the fingerprint or in the fingerprint population evolution.

Each fingerprint generated a single instrument response convoluted basis function for use in the GIPG fit. The resulting evolution of the population of the fingerprints appears in Fig. 9. The population of the monomer fingerprint appeared to decrease rapidly during the first 4 days of incubation. This contribution plateaued around day 8 and began to decrease again after day 24. The AggA fingerprint grew as the monomer disappeared and reached a maximum value on day 10. It then slowly decreased until day 18, after which it decreased more rapidly. The AggB fingerprint grew slowly beginning on day 6, pausing from days 12 to 16, after which it increased more rapidly, reaching a peak on day 24. The protofibril fingerprint was flat for the first 20 days of incubation, after which rapid growth occurred.

The evolution of the individual peak fits and fingerprints suggested three phases to the aggregation process: (1) the monomer converted to AggA, (2) then AggA converted into AggB, and (3) protofibrils began to appear after AggB had formed in large quantities.

ANS aggregation reversibility assay

One of the classic features of amyloid is its stability with respect to dissociation. To evaluate the amount of stabilization in different aggregates, we performed the ANS assay under conditions of 0.5 M urea concentration following incubation at 5 M urea. Under these conditions, unfolded monomers are expected to spontaneously refold. If the stabilization energy of the aggregate is greater than that of the refolding reaction, then the aggregation will not be reversible upon dilution of the denaturant.

The GIPG fit to the ANS aggregation reversibility assay data appears in Fig. 10. The nearly constant amplitude peak at 240 ps is consistent with free ANS in 0.5 M urea. This peak increases in amplitude during the first 5 days of incubation, decreases slightly until day 9, and then increases again, with the increase accelerating after day 14.

On day 0, the peak associated with surface binding at 830 ps did not appear at its 0.5 M control experiment position, suggesting that the association at this site was somewhat irreversible. From days 2 to 8, the peak was shifted to its reversible position at 1.1 ns; from days 10 to 18, it shifted to 790 ps. This result may indicate that there was a kinetic

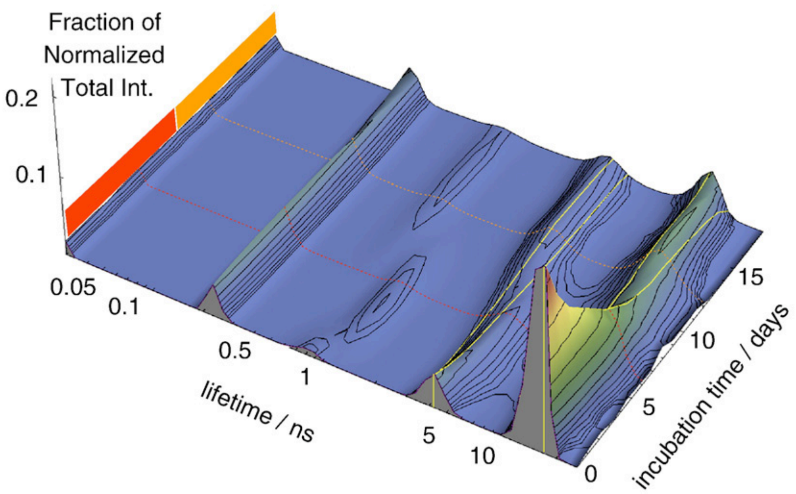

Fig. 10. GIPG fit for the ANS reversibility assay. The stability of the monomer and aggregate species is evaluated by reintroducing the incubated sample to a low-urea condition. Yellow mesh lines demarcate 3.6, 4.3, 13, and 16 ns to emphasize the loss–gain of species more clearly. The most dramatic feature is the nearly 50% loss of the 16-ns species, presumably the calyx-bound ANS, by day 8. The loss contemporaneously matches the change from the 4.3- to the 3.6-ns species. The χ^2_r for the global fit was 1.002.

competition between refolding of the surface site (perhaps at the α-helix) and binding of ANS. If this is the case, it would suggest that, during days 2–8, the binding site was protected from ANS until after refolding had occurred. The overall amplitude of this peak did not change much, consistent with the results of the standard ANS assay.

The peak at 16 ns was consistent with binding to the calyx; it decreased rapidly from days 0 to 4 and continued to decrease more slowly from days 6 to 12. This peak was replaced by a feature at 14 ns that appeared around day 1, increased until day 14, and decreased thereafter. Around day 18, the peak shifted to 13 ns. The rapid decrease in the availability of the calyx suggests that the aggregates in the early stages prevented the binding of ANS to the calyx. The shifts in lifetime suggest that although some structure resembling a calyx can reform as late as day 18, the population of these proteins is substantially reduced and they cannot reform the full calyx that is possible before aggregation has occurred.

We attributed the peak at 4.3 ns to the outer calyx binding site. This lifetime was shorter than the 5.4-ns lifetime that we determined from the 0.5 M control measurement. This suggests a degree of irreversibility even on day 0 in this binding site. This feature decreased from days 0 to 4, leveled out from days 5 to 8, and then decayed away from days 8 to 12. This feature was replaced by a peak at 3.6 ns that increased until day 12, after which it remained steady from 14 to 18 days. Overall, the qualitative behavior of this feature was similar to the feature at 16 ns.

There were essentially three manifestations of irreversibility represented in these data. The first was the ability of the protein to regain the same ANS binding sites after dilution from 5 to 0.5 M urea, as determined by the lifetime distribution. The dilution was performed in the presence of ANS. If the ANS binds to the site in question prior to refolding, then it could lock the protein into a misfolded conformation at the binding site. The result is a lifetime that more closely resembles the 5 M urea control experiment conditions than the 0.5 M urea conditions. The second type of irreversibility was the loss of a particular binding site as aggregation progressed. This suggests that the aggregate disrupts or blocks access to the site in question and that the site cannot be reformed by dilution of the denaturant. The third type of irreversibility was the replacement of one site with another. This is similar to the second type of irreversibility, except that the structural change has resulted in a new local environment for the binding of ANS.

These three types of irreversibility suggest that there are two main stages to the incubation over the range of 0–18 days that appear to transition at 8–10 days. The changes that were reflected in the irreversibility suggested that one of the key elements distinguishing the different aggregation steps was the reversibility of the interactions between monomers in the different aggregates.

Discussion

Conformational lability prior to incubation

Our results suggest that β-LGa was conformationally labile under the amyloidogenic incubation conditions. The ThT assay showed little change in signal over the protein-free control, except for an additional peak at 110 ps. The ANS assay showed several lifetime components and a substantial contribution from intact calyx binding of ANS, suggesting that ANS may be stabilizing the folded structure.[78] The multiplicity of features in the 5 M urea ANS assay suggested multiple structures for monomeric β-LGa. In particular, the calyx or hydrophobic core was more flexible and more accessible to solvent, as shown by ANS fluorescence. The reversibility ANS assay showed minor signs of irreversibility and fewer lifetime features. Under these conditions, β-LGa adsorbed on an aminosilanized mica surface and appeared to be denatured.

The DLS measurements showed that the protein had swelled and had a broad distribution of hydrodynamic radius. In a titration from 0 to 7 M urea, the width of the DLS R_H distribution was broadest at 5 M urea. That the width of the distribution is resolvable implied that the exchange time within that distribution was longer than the characteristic diffusion time of ~20 μs. Amyloid formation from β-LGa has been observed to be fastest at 5 M urea.[13] The day 0 DLS results showed that the conditions giving the maximum rate of amyloidogenesis were coincident with those that created the maximum variance in the hydrodynamic radius of β-LGa.

Overall, we can conclude that there are multiple monomeric structures exchanging in the sample under these conditions. The partially folded intermediate appeared to be the aggregation-prone state. The ability to exchange between multiple conformations may be a crucial feature in determining aggregation propensity. To use free-energy landscape language, the folding funnel flattens, allowing access to disordered states of increased R_H and core solvation.

Early lag-phase aggregation was more reversible

The DLS assay showed that aggregation occurs in the first few days of incubation, with average particle sizes passing through a dimeric stage to a steady state with an average size consistent with that of tetramers. In the AFM assay, the aggregates could be imaged on a clean mica surface; however, on a more strongly adsorbing aminosilanized mica surface, the aggregates were disrupted and denatured on the surface. The ANS 5 M urea assay revealed a decreased ability of ANS to bind to the calyx. The irreversibility assay showed changes predominantly in the calyx binding site. The fingerprint analysis of the ANS 5 M urea assay suggested that a new species was growing, with a small contribution from another species. We call these species AggA and AggB, respectively. The differences in fingerprints suggested changes in the nature and relative populations of different binding sites and, therefore, a change in the tertiary structure of the monomers upon aggregation. However, the ThT assay only showed small changes in lifetime distribution, implying that this structural change did not occur in the cross-β structure associated with amyloid.

The stabilization energy of AggA was less than the electrostatic interaction with the aminosilanized mica surface. However, AggA was not disrupted by dilution into more native-like conditions, suggesting that the AggA stabilization energy was between the folding energy and the surface adsorption energy. The interaction between monomers in AggA most likely involved some change or disruption of the calyx that allowed solvent access. Some parts of the structural changes that occurred upon AggA formation were still reversible at this stage. This suggested that the structure of β-LGa in AggA more closely resembled the free monomer than did AggB. AggA appeared to be limited in total size. Continued growth most likely required disruption of the remaining free-monomer-like structure. AggA in Fig. 11 was modeled with swapping of structural elements. This type of interaction is possible because of the inherent self-complimentary nature of folded proteins. These interactions are also likely to sterically limit the maximum size of aggregates that could be so assembled.

Late lag-phase aggregation loses calyx

During the late lag phase, small aggregates could be possibly imaged on the aminosilanized mica surface. In the DLS assay, the appearance of a wing on the distribution to larger R_H and the growth of a new feature at large R_H suggest that aggregate growth resumes during this stage. The ThT assay shows a new pattern in the lifetime distribution. The ANS fingerprint analysis showed that AggB begins to get appreciable population, while AggA decreases in population, suggesting a conversion from AggA to AggB. The ANS irreversibility assay showed that AggB had new binding sites for ANS. This suggested that the structural conversion was inside of the aggregate, rather than a newly formed aggregate.

Conversion to AggB appeared to be required for growth to continue. The stability of AggB with respect to dissociation on the aminosilanized surface implied that it was more stable than AggA. AggB was larger, on average, than AggA. The monomer

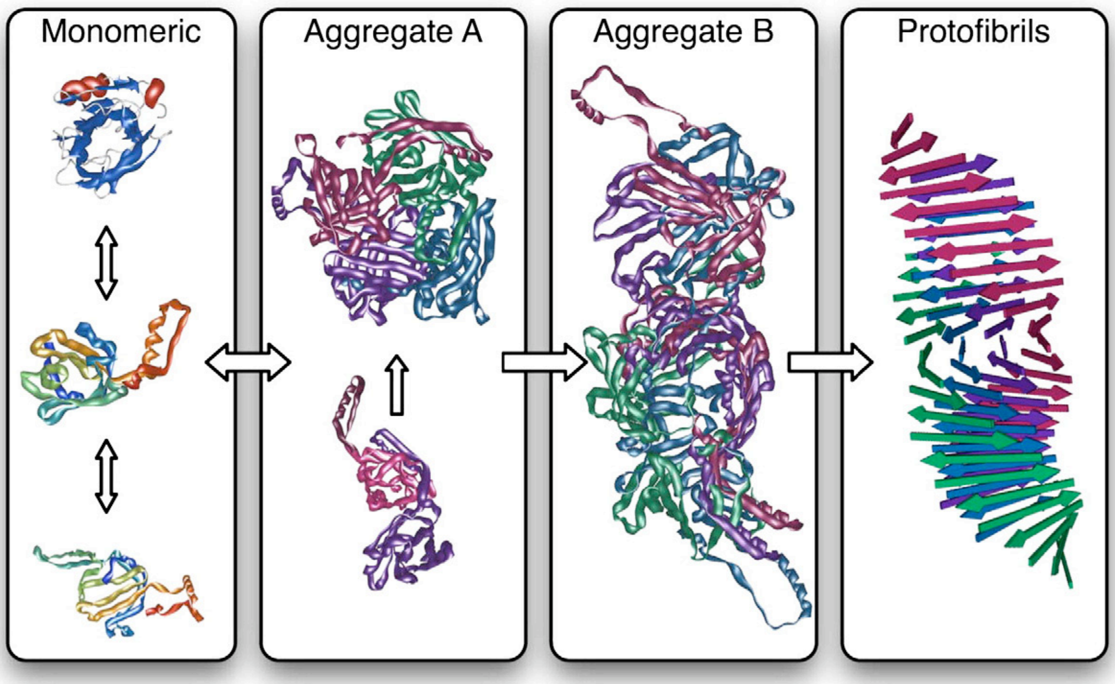

Fig. 11. Proposed mechanism of β-LGa aggregation. Amyloidogenic conditions put β-LGa into a disordered, conformationally labile state that reversibly aggregates into dimers and tetramers that are stabilized in part by hydrophobic interactions. The calyx is intact but structurally altered. As aggregation continues, the calyx is lost, and the loosely associated oligomers convert into higher-order more stable aggregates. These aggregates then convert into protofibrils that elongate in the classic growth phase of sigmoidal kinetics. Monomeric: The top is the folded monomer; the middle was obtained by modeling the unfolding of the C-terminal α-helix and β-strand I. The bottom was obtained by flattening the barrel into a sheet. AggA: These oligomers were obtained by aligning complementary surfaces of the middle monomer structure. Aggregate B: This octamer was modeled by stacking the flattened monomer structure into four layers. Protofibrils: Four sheets of the canonical cross-β structure.

structure changed from AggA to AggB, as reflected in the changes in the ANS assay binding sites. AggB was also structurally different from AggA in terms of the monomer–monomer interactions, as suggested by the ANS reversibility assay. The changes in AggB structure allowed ThT–ThT interactions that were not possible in AggA. The ThT assay implied that some elements of the AggB structure might be similar to those in amyloid fibril. However, no fibrils or protofibrils were observed at this stage. The ThT lifetime contributions of fibrillar species were different from those of AggB. Conversion into AggB could be misinterpreted as amyloid formation if only changes in ThT intensity were measured.

Protofibrils appear after day 20

During the growth phase, the light-scattering intensity increased enormously and the amount of large aggregate increased. AFM images showed the appearance of protofibrils followed by elongation of protofibrils and, finally, fibril assembly into long fibrils of varying lengths and diameters. The ANS assay showed dramatic growth in the protofibril fingerprint, a decrease in the AggA fingerprint, and a steady state for the AggB fingerprint. At very long incubation times, very little ANS binding to mature fibrils was observed, suggesting the presence of accessible hydrophobic regions on the protofibrils that disappeared upon formation of mature fibrils. We speculate that these hydrophobic locations are involved in the lateral association of protofibrils into fibrils. The ThT assay showed a new lifetime distribution pattern that continued to grow until at least day 34. We associated this pattern with amyloid protofibrils, since the distribution was still very different from that observed from mature fibrils. Only some of the protofibril features were present in the ThT assay (where mature fibrils were present) taken after 2 months of incubation. A large ThT lifetime contribution that was not present at any other stage was present in the mature fibril data. The structure of protofibrils at the ThT binding level must be different from that of fibrils.

Overall mechanism

The native β-strands in β-LGa are not in the right orientation to attain the cross-β geometry. It appears likely that an interaction analogous to domain swapping or opening of the β-sheet "sandwich" would be required for β-LGa to associate with the cross-β geometry. Based on the observed morphology of amyloid fibrils and the size of β-LGa, it would require approximately two to three β-LGa monomers, or four to six flattened monomers, to form the transverse structure of a 4- to 5-nm-diameter fibril. A fibril ~45 nm long would contain ~32 β-LGa monomers and would have a total molecular mass of 590 kDa. A fully formed amyloid fibril of 10 nm×200 nm would contain ~700 β-LGa monomers and would have a total molecular mass of 12.9 MDa.

Our results suggest that there are two parts to the lag phase of β-LGa amyloid formation. The sequence of events is similar to some recent kinetic analyses of amyloid nucleation.[22] We monitored the role of the hydrophobic core using the signature lifetime of ANS in the calyx. We showed how fluorescence lifetime fingerprints can be used to extract the contribution of multiple species during incubation. We identified two intermediates in the lag phase that are distinguishable by their relative stability, size, and binding of ThT and ANS. ANS is sensitive to the rigidity and polarity of binding locations, while ThT is sensitive to the relative geometry of its ThT binding sites. Based on this information, we must conclude that significant rearrangement of structure must occur between AggA and AggB. The standard interpretation of this change would be that AggB represents the conversion into the amyloid nucleus. However, ThT gave different signals when bound to AggA, AggB, and protofibrils. Moreover, the onset of the rapid growth of protofibrils does not occur until many days after the appearance of AggB. Therefore, we must conclude that AggB is distinct in structure from both AggA and protofibrils. The presence of multiple aggregated species in a serial mechanism suggests that homogenous nucleation may not be a universal description of amyloid formation kinetics.

The initial aggregation into AggA and the subsequent aggregation into AggB must have some driving force associated with them. Two simple models—colloidal aggregation and polymer phase stability—can be invoked to frame the initial aggregation. The inherent hydrophobicity of the polypeptide chain can lead to an aggregated phase of protein being more stable.[16] The driving force in this case is the increased number of favorable protein–protein and water–water contacts and a decreased number of protein–water contacts. Colloidal aggregation is similar, except that it attributes the driving force to the partitioning of amino acids with unfavorable protein–water contact energies into a region of higher protein–protein contacts, while amino acids with favorable protein–water contact energies are partitioned into the surface of the aggregate. This partitioning puts an additional geometric constraint on the aggregation process that is not present in the phase-stability picture.

Given the large number of charged amino acids on β-LGa, we favor the colloidal aggregation picture; however, our data only indirectly address this issue. Colloidal association in AggA and then in AggB could reduce the barrier to the conformational change in cross-β required to form amyloid. Colloidal association is required because the monomer cannot rearrange without sacrificing a prohibitively large number of hydrophobic interactions. If the protein has a strong hydrophobic core, then the hydrophobic effect is too strong to disrupt. If the protein is completely unfolded, the possible hydrophobic gains are too weak to overcome the translational entropy that is lost to aggregation.

There is a connection to protein folding in this analysis. Proteins below a certain size typically cannot fold stably. This can be attributed to the absence of a large enough number of favorable interactions to meet the thermodynamic conditions of cooperativity. By associating with colloidal or phase-separated aggregates, the protein increases its effective molecular weight and potential number of favorable interactions to the point where the fold of amyloid is accessible. This colloidal or phase-separated promotion of conformational rearrangement may explain the ability of surfactants to promote amyloid formation.

Amyloidogenic conditions have been identified for many non-disease-related proteins. This leads to the hypothesis that aggregation of proteins leading to amyloid fibril formation is a generic feature of polypeptides.[7,79] If the hypothesis that amyloidogenesis is a generic possibility for proteins is valid, then we should think about amyloid as a particular state of protein in the polypeptide phase diagram. The driving forces for phase separation into amyloid should depend on the relative contributions of hydrogen bonding to the cross-β structure and the arrangement of hydrophobic groups. There is evidence that the polypeptide is hydrophobic from a polymer physics point of view, i.e., that polymer–polymer contacts are more energetically favorable than polymer–water contacts.[80,81] This would suggest that the environmental and sequence determinants for amyloid propensity are more based on the lowering of the barrier to formation of the amyloid phase than on the stability of the amyloid phase itself. In other words, the effects are principally kinetic rather than thermodynamic. In particular, in this study, we propose that the initial aggregation to AggA allows a larger hydrophobic core to be formed in AggB. This allows the cross-β structure to be obtained in the protofibril. The initial bistability of the monomer allows formation of AggA. AggA allows a lower-barrier pathway to the formation of AggB, which is large enough to rearrange into the more stable cross-β structure without a prohibitively large activation barrier. This allows the spontaneous formation of amyloid protofibrils to occur even when barriers to the formation of the cross-β structure directly from the monomer or even AggA are energetically prohibitive.

Materials and Methods

Materials

Lyophilized β-LGa, ThT, urea, aminopropyltriethoxysilane (APTES), and dibasic and monobasic sodium phosphate were purchased from Sigma. Fluorescence-grade ANS was purchased from Fluka.

A 10 mM sodium phosphate (pH 7.0) stock buffer solution was prepared with HPLC-grade water. This buffer was used to prepare a second stock buffer containing 7.5 M urea. Both stock buffers were filtered through a 0.22-μm polyethersulfone filter and stored at 4 °C. For DLS measurements, extra care was taken to minimize scattering from dust contaminants by filtering stock buffer solutions with a prewashed 0.020-μm syringe filter (Whatman). The 0 M urea stock phosphate buffer was used to prepare a 138 μM stock protein solution of β-LGa, which was stored at 4 °C. The protein stock solution was checked by UV absorption every few days to ensure its stability.

β-LGa incubations

We incubated β-LGa under conditions previously reported to show maximum amyloidogenicity,[13] and we aliquoted samples for time-resolved ANS and ThT luminescence, DLS, and AFM experiments.

For time-resolved luminescence and DLS measurements, 1.5 mL of protein sample for incubation was prepared every other day for 28 days and used for ANS assay along with the long-term DLS experiments. For ThT and ANS reversibility assay, samples were prepared every day for 34 days and 18 days, respectively. Each incubation sample was prepared by combining a 500-μL aliquot of the stock protein solution with 1000 μL of the 7.5 M urea stock solution in a polypropylene Eppendorf tube, resulting in a final protein concentration of 46 μM and a final urea concentration of 5 M. The sample was capped, sealed with Parafilm, and placed in an incubator at 37 °C. At the conclusion of the incubation, all samples were breached and each was parsed for contemporaneous experimentation.

To investigate the earliest aggregation with DLS, a sample of 46 μM β-LGa in 5 M urea and 10 mM sodium phosphate (pH 7.0) was prepared from the stock solutions above. The sample filled the cuvette to approximately 90% capacity in order to reduce the sample headspace. DLS was measured while simultaneously incubated at 37 °C in a Peltier sample chamber (instrumentation discussed below).

For the AFM measurements, lyophilized β-LGa was reconstituted and dialyzed against prefiltered (0.22 μm) 100 mM phosphate buffer (pH 7.0). Prefiltered concentrated urea buffer was added, which resulted in a final sample condition for incubation of 50 μM protein in 5 M urea and 13.7 mM sodium phosphate (pH 7.0). The sample was incubated in a Parafilm-sealed 1.5-mL Eppendorf tube at 37 °C over 65 days. The sample was inverted once on each day that AFM was measured, and 20 μL was aliquoted for the AFM image.

Time-resolved luminescence

Time-resolved luminescence was measured by time-correlated single-photon counting (TCSPC). The Experimental setup has been previously described,[82] with the exception that the Spectra Physics Tsunami Ti:Sapphire laser was operated in femtosecond mode. All samples were analyzed at 37 °C in a Quantum Northwest (Spokane, WA) TLC150 Peltier controller sample chamber.

For the ThT assay, a stock 5 μM ThT solution was prepared from the 0 M urea stock buffer. Fifty microliters of an incubated time point was aliquoted into 450 μL of ThT solution in a reduced volume cuvette and allowed to stand for 15 min at 37 °C. The excitation laser was tuned to 450 nm, and the luminescence was observed at 482 nm. The time-zero intensity ranged between 30,000 and 60,000 photons. A 50-ns collection window was used. Instrument response functions typically had a full width at half-maximum of approximately 90 ps.

An 80 μM ANS stock solution was prepared in a 0 M urea stock buffer for the ANS assay. Five hundred microliters of an incubated time point was combined with 10 μL of the ANS stock solution and allowed to stand for 15 min at 37 °C.

For the ANS reversibility assay, a 1 μM ANS stock solution was prepared in a 0 M urea stock buffer. Fifty microliters of an incubated time point was combined with 450 μL of the ANS stock solution and allowed to stand for 15 min at 37 °C. Excitation beam was tuned to 390 nm, and the fluorescence emission was observed at 485 nm over 100- and 82-ns collection windows for the ANS and ANS reversibility assays, respectively. A typical transient's time-zero intensity was 4000 photons for the ANS reversibility assay, whereas an intensity of 18,000 photons was common for the ANS assay. Instrument response functions typically had a full width at half-maximum of approximately 100 ps.

We expect the population of the luminescent species to be piecewise continuous with respect to incubation time, making this system a prime candidate for global data analysis by the GIPG method.[64,82] ThT luminescence lifetime distributions were fitted on an 80-point grid, logarithmically spaced in lifetime ranging from 0.002 to 20 ns. Both types of ANS assays were fitted on their own 58-point grid, logarithmically spaced in lifetime ranging from 0.03 to 30 ns. A baseline and scattering term was included in the fits. To compensate for potential incident laser intensity fluctuations across incubation time, all TCSPC transients were normalized by the total time-zero photon population. This is accomplished by summing the parameters from a nonnegative least squares fit.[64,83] The GIPG fits were considered statistically indistinguishable from the local fits by calculating the probability to reject[64,84] to be $<10^{-4}$ for all fits. ThT, ANS, and ANS reversibility assays of GIPG fits used 8×10^5, 1×10^6, and 1.5×10^6 iterations, respectively. The GIPG step scaling term referred to as λ was set to 0.9. GIPG algorithm can be obtained from the website† as an Igor Pro 6.03 procedure file.

Dynamic light scattering

Fluctuations of scattered light intensity were measured using a homodyne technique. At a particular incubation time x, the intensity correlation function $g_2(t,x)$ was measured by a modified Nicomp Model 380 Particle Size Analyzer (Particle Sizing Systems). Scattered light from the incident laser ($\lambda=532$ nm) was collected orthogonally ($\theta=90°$). The system employs a linearly scaled 64-channel digital autocorrelator. For experiments completed in this study, the native autocorrelator was bypassed by an ALV-6010 Multi-Tau autocorrelator (ALV GmbH, Langen, Germany) for the maximum possible statistical accuracy across several orders of magnitude in decay time.[85]

Round borosilicate glass cuvettes (Kimble Glass) were used for all DLS measurements. In order to minimize dust contamination, each cuvette was rinsed with Millipore water. Cuvettes were placed in a microcentrifuge, inverted (open side face down), then spun dry and stored face down. After the sample had been quickly and carefully added to the cuvette, it was covered with transparent tape to keep it dust-free, then wrapped in Parafilm for an additional seal.

For the 28-day DLS study, 250 μL of incubated sample was placed in a clean dry cuvette. Twenty correlation functions were measured sequentially for 30 s apiece for each incubated sample. The cuvette chamber was held at a constant temperature of 37 °C. For the continuous-acquisition incubation, the same sample was analyzed every 15 min for 5 min at 37 °C for 4.7 days.

The distribution of decay rates $f(\Gamma,x)$ for a particular incubation time point x is related to the field correlation function $g_1(t,x)$ by:

$$g_1(t,x) = \int_0^\infty e^{-\Gamma t} f(\Gamma,x)\mathrm{d}\Gamma \tag{1}$$

where $f(\Gamma,x)$ can be solved for by the inverse Laplace transform. In most cases, the intensity and field correlation functions can be related via the Siegert relation, such that $\sqrt{g_2(t,x)-1}\propto g_1(t,x)$.[85]

GIPG was originally demonstrated by globally fitting TCSPC transients, but it can be also employed to globally fit many types of spectroscopic data that require an inverse Laplace transform, such as in Eq. (1), as long as there is piecewise continuity in the experimental domain x. One difference is that the intensity correlation functions do not require instrument response convolution of the basis set. Another difference is that the standard deviations for the data were calculated in real time by the ALV-6010 correlator using a noise model.

DLS data were globally fitted onto a 50-point grid with logarithmically spaced decay times Γ^{-1} ranging from 0.001 to 65 ms. A baseline term was included. The total number of correlation functions used in the short-term DLS fit was reduced from 340 to 34 by averaging every 10 correlation functions into a single trace and by propagating the error accordingly. The probability to reject the GIPG solution for both data sets was $<10^{-4}$.

In DLS, a particle's decay time is related to the translational diffusion constant through the scattering vector $\mathbf{q}$, such that $D=\Gamma/\mathbf{q}^2$, where $\mathbf{q}=4\pi/\lambda \sin(\theta/2)$. The diffusion constant can then be converted into Stokes hydrodynamic radius (R_H) using the Stokes–Einstein relation $R_H=(k_BT)/(6\pi\eta_0 D)$, assuming a spherical shape. For these experiments, T is the temperature, η_0 is the refractive index of the buffer, and k_B is the Boltzmann constant. The characteristic density of the partially unfolded monomer determined from assignment of a urea titration DLS experiment at 5.0 M was used to scale the oligomer sizes.

Atomic force microscopy

To obtain better adhesion of protein aggregates to a mica surface, chemical surface modification was implemented. Twenty microliters of 0.1 (vol/vol) APTES was applied evenly on a freshly cleaved 9.9-mm-diameter mica disk. After 10 min, unreacted APTES was rinsed away with 15 mL of 0.2 μM filtered deionized water. The surface was blown dry with high-purity compressed nitrogen gas. Incubated sample was applied evenly on a freshly prepared surface for 10 min. Unbound species were rinsed away with Millipore water. The sample was again dried with nitrogen gas before being imaged with a MultiMode Scanning Probe Microscope (Digital Instruments) with a TESP tip in tapping mode.

† http://talaga.rutgers.edu

Acknowledgements

This work was supported by grant R01GM071684 from the National Institutes of Health. J.T.G. was supported by a Graduate Assistantship in Areas of

National Need grant to the Department of Chemistry and Chemical Biology. We thank Ben Strangfeld for assisting with the DLS experiments, Troy Messina for IMPACT minimizations, and Richard Ebright for the use of the atomic force microscope.

References

1. Sipe, J. D. & Cohen, A. S. (2000). Review: history of the amyloid fibril. *J. Struct. Biol.* **130**, 88–98.
2. Walsh, D. M., Hartley, D. M. & Selkoe, D. J. (2003). The many faces of aβ: structures and activity. *Curr. Med. Chem. Immunol. Endocr. Metab. Agents*, **3**, 277–291.
3. Wetzel, R. (2002). Ideas of order for amyloid fibril structure. *Structure*, **10**, 1031–1036.
4. Solomon, B. (2002). Towards Alzheimer's disease vaccination. *Mini-Rev. Med. Chem.* **2**, 85–92.
5. Kirkitadze, M. D., Bitan, G. & Teplow, D. B. (2002). Paradigm shifts in Alzheimer's disease and other neurodegenerative disorders: the emerging role of oligomeric assemblies. *J. Neurosci. Res.* **69**, 567–577.
6. Hardy, J. & Selkoe, D. J. (2002). The amyloid hypothesis of Alzheimer's disease: progress and problems on the road to therapeutics. *Science*, **297**, 353–356.
7. Chiti, F. & Dobson, C. (2006). Protein misfolding, functional amyloid, and human disease. *Annu. Rev. Biochem.* **75**, 333–366.
8. Teplow, D. B. (1998). Structural and kinetic features of amyloid β-protein fibrillogenesis. *Amyloid*, **5**, 121–142.
9. Rochet, J.-C., Lansbury, J. & Peter, T. (2000). Amyloid fibrillogenesis: themes and variations. *Curr. Opin. Struct. Biol.* **10**, 60–68.
10. Murphy, R. M. & Pallitto, M. M. (2000). Probing the kinetics of β-amyloid self-association. *J. Struct. Biol.* **130**, 109–122.
11. Zerovnik, E. (2002). Amyloid-fibril formation. Proposed mechanisms and relevance to conformational disease. *Eur. J. Biochem.* **269**, 3362–3371.
12. Nielsen, L., Khurana, R., Coats, A., Frokjaer, S., Brange, J. & Vyas, S. (2001). Effect of environmental factors on the kinetics of insulin fibril formation: elucidation of the molecular mechanism. *Biochemistry*, **40**, 6036–6046.
13. Hamada, D. & Dobson, C. M. (2002). A kinetic study of β-lactoglobulin amyloid fibril formation promoted by urea. *Protein Sci.* **11**, 2417–2426.
14. Lee, C.-C., Nayak, A., Sethuraman, A., Belfort, G. & McRae, G. J. (2007). A three-stage kinetic model of amyloid fibrillation. *Biophys. J.* **92**, 3448–3458.
15. Lomakin, A., Teplow, D. B., Kirschner, D. A. & Benedek, G. B. (1997). Kinetic theory of fibrillogenesis of amyloid β-protein. *Proc. Natl Acad. Sci. USA*, **94**, 7942–7947.
16. Pappu, R. V., Wang, X., Vitalis, A. & Crick, S. L. (2008). A polymer physics perspective on driving forces and mechanisms for protein aggregation. *Arch. Biochem. Biophys.* **469**, 132–141.
17. Pallitto, M. M. & Murphy, R. M. (2001). A mathematical model of the kinetics of β-amyloid fibril growth from the denatured state. *Biophys. J.* **81**, 1805–1822.
18. Kayed, R., Head, E., Thompson, J. L., McIntire, T. M., Milton, S. C., Cotman, C. W. & Glabe, C. G. (2003). Common structure of soluble amyloid oligomers implies common mechanism of pathogenesis. *Science*, **300**, 486–489.
19. Kane, M. D., Lipinski, W. J., Callahan, M. J., Bian, F., Durham, R. A., Schwarz, R. D. *et al.* (2000). Evidence for seeding of β-amyloid by intracerebral infusion of Alzheimer brain extracts in β-amyloid precursor protein-transgenic mice. *J. Neurosci.* **20**, 3606–3611.
20. Harper, J. D. & Lansbury, P. T., Jr (1997). Models of amyloid seeding in Alzheimer's disease and scrapie: mechanistic truths and physiological consequences of the time-dependent solubility of amyloid proteins. *Annu. Rev. Biochem.* **66**, 385–407.
21. Stöhr, J., Weinmann, N., Wille, H., Kaimann, T., Nagel-Steger, L., Birkmann, E. *et al.* (2008). Mechanisms of prion protein assembly into amyloid. *Proc. Natl Acad. Sci. USA*, **105**, 2409–2414.
22. Andrews, J. M. & Roberts, C. J. (2007). A Lumry–Eyring nucleated polymerization model of protein aggregation kinetics: 1. Aggregation with pre-equilibrated unfolding. *J. Phys. Chem. B*, **111**, 7897–7913.
23. Goldsbury, C., Kistler, J., Aebi, U., Arvinte, T. & Cooper, G. J. S. (1999). Watching amyloid fibrils grow by time-lapse atomic force microscopy. *J. Mol. Biol.* **285**, 33–39.
24. Stolz, M., Stoffler, D., Aebi, U. & Goldsbury, C. (2000). Monitoring biomolecular interactions by time-lapse atomic force microscopy. *J. Struct. Biol.* **131**, 171–180.
25. Gosal, W. S., Clark, A. H., Pudney, P. D. A. & Ross-Murphy, S. B. (2002). Novel amyloid fibrillar networks derived from a globular protein: β-lactoglobulin. *Langmuir*, **18**, 7174–7181.
26. Parbhu, A., Lin, H., Thimm, J. & Lal, R. (2002). Imaging real-time aggregation of amyloid β protein (1–42) by atomic force microscopy. *Peptides*, **23**, 1265–1270.
27. Kusumoto, Y., Lomakin, A., Teplow, D. B. & Benedek, G. B. (1998). Temperature dependence of amyloid β-protein fibrillization. *Proc. Natl Acad. Sci. USA*, **95**, 12277–12282.
28. Bergasa-Caceres, F. & Rabitz, H. A. (2003). Two-state folding kinetics of small proteins in the sequential collapse model: dependence of the folding rate on contact order and temperature. *J. Phys. Chem. B*, **107**, 12874–12877.
29. Prusiner, S. B. (1982). Novel proteinaceous infectious particles cause scrapie. *Science*, **216**, 136–144.
30. Griffith, J. S. (1967). Self-replication and scrapie. *Nature*, **215**, 1043–1044.
31. Schenk, D. (2002). Opinion: amyloid-β immunotherapy for Alzheimer's disease: the end of the beginning. *Nat. Rev. Neurosci.* **3**, 824–828.
32. Satheeshkumar, K. S. & Jayakumar, R. (2003). Conformational polymorphism of the amyloidogenic peptide homologous to residues 113–127 of the prion protein. *Biophys. J.* **85**, 473–483.
33. Bouchard, M., Zurdo, J., Nettleton, E. J., Dobson, C. M. & Robinson, C. V. (2000). Formation of insulin amyloid fibrils followed by FTIR simultaneously with CD and electron microscopy. *Protein Sci.* **9**, 1960–1967.
34. Lansbury, J., Peter, T., Costa, P. R., Griffiths, J. M., Simon, E. J., Auger, M. *et al.* (1995). Structural model for the β-amyloid fibril based on interstrand alignment of an antiparallel-sheet comprising a C-terminal peptide. *Nat. Struct. Biol.* **2**, 990–998.
35. Chiti, F., Webster, P., Taddei, N., Clark, A., Stefani, M., Ramponi, G. & Dobson, C. M. (1999). Designing conditions for *in vitro* formation of amyloid protofilaments and fibrils. *Proc. Natl Acad. Sci. USA*, **96**, 3590–3594.
36. Abe, H. & Nakanishi, H. (2003). Novel observation of

a circular dichroism band originating from amyloid fibril. *Anal. Sci.* **19**, 171–173.

37. Carrotta, R., Bauer, R., Waninge, R. & Rischel, C. (2001). Conformational characterization of oligomeric intermediates and aggregates in β-lactoglobulin heat aggregation. *Protein Sci.* **10**, 1312–1318.
38. Baskakov, I. V., Legname, G., Baldwin, M. A., Prusiner, S. B. & Cohen, F. E. (2002). Pathway complexity of prion protein assembly into amyloid. *J. Biol. Chem.* **277**, 21140–21148.
39. Quintas, A., Saraiva, M. J. & Brito, R. M. (1999). The tetrameric protein transthyretin dissociates to a non-native monomer in solution. A novel model for amyloidogenesis. *J. Biol. Chem.* **274**, 32943–32949.
40. Safar, J., Roller, P. P., Gajdusek, D. C. & Gibbs, C. J., Jr (1994). Scrapie amyloid (prion) protein has the conformational characteristics of an aggregated molten globule folding intermediate. *Biochemistry*, **33**, 8375–8383.
41. Srisailam, S., Kumar, T. K., Rajalingam, D., Kathir, K. M., Sheu, H.-S., Jan, F.-J. *et al.* (2003). Amyloid-like fibril formation in an all β-barrel protein. Partially structured intermediate state(s) is a precursor for fibril formation. *J. Biol. Chem.* **278**, 17701–17709.
42. Gorman, P. M. & Chakrabartty, A. (2001). Alzheimer β-amyloid peptides: structures of amyloid fibrils and alternate aggregation products. *Biopolymers*, **60**, 381–394.
43. Huang, T. H. J., Yang, D.-S., Fraser, P. E. & Chakrabartty, A. (2000). Alternate aggregation pathways of the Alzheimer β-amyloid peptide. An *in vitro* model of preamyloid. *J. Biol. Chem.* **275**, 36436–36440.
44. Banks, J. L., Beard, H. S., Cao, Y., Cho, A. E., Damm, W., Farid, R. *et al.* (2005). Integrated modeling program, applied chemical theory (IMPACT). *J. Comput. Chem.* **26**, 1752–1780.
45. Uhrinova, S., Smith, M. H., Jameson, G. B., Uhrin, D., Sawyer, L. & Barlow, P. N. (2000). Structural changes accompanying pH-induced dissociation of the β-lactoglobulin dimer. *Biochemistry*, **39**, 3565–3574.
46. Sawyer, L. & Kontopidis, G. (2000). The core lipocalin, bovine β-lactoglobulin. *Biochim. Biophys. Acta*, **1482**, 136–148.
47. Sagis, L. M. C., Veerman, C. & Van der Linden, E. (2004). Mesoscopic properties of semiflexible amyloid fibrils. *Langmuir*, **20**, 924–927.
48. Buck, M. (1998). Trifluoroethanol and colleagues: cosolvents come of age. Recent studies with peptides and proteins. *Q. Rev. Biophys.* **31**, 297–355.
49. Chikenji, G. & Kikuchi, M. (2000). What is the role of non-native intermediates of β-lactoglobulin in protein folding? *Proc. Natl Acad. Sci. USA*, **97**, 14273–14277.
50. Forge, V., Hoshino, M., Kuwata, K., Arai, M., Kuwajima, K., Batt, C. A. & Goto, Y. (2000). Is folding of β-lactoglobulin non-hierarchic? Intermediate with native-like β-sheet and non-native α-helix. *J. Mol. Biol.* **296**, 1039–1051.
51. Hamada, D. & Goto, Y. (1997). The equilibrium intermediate of β-lactoglobulin with non-native α-helical structure. *J. Mol. Biol.* **269**, 479–487.
52. Hamada, D., Segawa, S.-I. & Goto, Y. (1996). Non-native α-helical intermediate in the refolding of β-lactoglobulin, a predominantly β-sheet protein. *Nat. Struct. Biol.* **3**, 868–873.
53. Kuwata, K., Hoshino, M., Era, S., Batt, C. A. & Goto, Y. (1998). $\alpha \rightarrow \beta$ transition of β-lactoglobulin as evidenced by heteronuclear NMR. *J. Mol. Biol.* **283**, 731–739.
54. Bergasa-Caceres, F. & Rabitz, H. A. (2003). Sequential collapse folding pathway of β-lactoglobulin: parallel pathways and non-native secondary structure. *J. Phys. Chem. B*, **107**, 3606–3612.
55. Kuwajima, K., Yamaya, H. & Sugai, S. (1996). The burst-phase intermediate in the refolding of β-lactoglobulin studied by stopped-flow circular dichroism and absorption spectroscopy. *J. Mol. Biol.* **264**, 806–822.
56. Kuwata, K., Shastry, R., Cheng, H., Hoshino, M., Batt, C. A., Goto, Y. & Roder, H. (2001). Structural and kinetic characterization of early folding events in β-lactoglobulin. *Nat. Struct. Biol.* **8**, 151–155.
57. Kella, N. K. & Kinsella, J. E. (1988). Structural stability of β-lactoglobulin in the presence of kosmotropic salts. A kinetic and thermodynamic study. *Int. J. Pept. Protein Res.* **32**, 396–405.
58. Creamer, L. K. (1995). Effect of sodium dodecyl sulfate and palmitic acid on the equilibrium unfolding of bovine β-lactoglobulin? *Biochemistry*, **34**, 7170–7176.
59. D'Alfonso, L., Collini, M. & Baldini, G. (2003). Trehalose influence on β-lactoglobulin stability and hydration by time resolved fluorescence. *Eur. J. Biochem.* **270**, 2497–2504.
60. Kirk, W., Kurian, E. & Wessels, W. (2007). Photophysics of ANS v. decay modes of ANS in proteins: the IFABP–ANS complex. *Biophys. Chem.* **125**, 50–58.
61. Gasymov, O. K., Abduragimov, A. R. & Glasgow, B. J. (2007). Characterization of fluorescence of ANS–tear lipocalin complex: evidence for multiple-binding modes. *Photochem. Photobiol.* **83**, 1405–1414.
62. Khurana, R., Gillespie, J. R., Talapatra, A., Minert, L. J., Ionescu-Zanetti, C., Millett, I. & Fink, A. L. (2001). Partially folded intermediates as critical precursors of light chain amyloid fibrils and amorphous aggregates. *Biochemistry*, **40**, 3525–3535.
63. Lindgren, M., Sorgjerd, K. & Hammarstromy, P. (2005). Detection and characterization of aggregates, prefibrillar amyloidogenic oligomers, and protofibrils using fluorescence spectroscopy. *Biophys. J.* **88**, 4200–4212.
64. Giurleo, J. T. & Talaga, D. S. (2008). Global fitting without a global model: regularization based on the continuity of the evolution of parameter distributions. *J. Chem. Phys.* **128**, 114114; (1–18).
65. Lomakin, A., Benedek, G. B. & Teplow, D. B. (1999). Monitoring protein assembly using quasielastic light scattering spectroscopy. *Methods Enzymol.* **309**, 429–459.
66. Modler, A. J., Gast, K., Lutsch, G. & Damaschun, G. (2003). Assembly of amyloid protofibrils via critical oligomers—a novel pathway of amyloid formation. *J. Mol. Biol.* **325**, 135–148.
67. Waldrop, F. S., Puchtler, H. & Meloan, S. N. (1984). Fluorescent thiazole stains for amyloid without differentiation. *J. Histotechnol.* **7**, 123–126.
68. Elhaddaoui, A., Delacourte, A. & Turrell, S. (1993). Spectroscopic study of Congo red and thioflavin binding to amyloid-like proteins. *J. Mol. Struct.* **294**, 115–118.
69. LeVine, H. (1995). Thioflavine T interaction with amyloid β-sheet structures. *Amyloid*, **2**, 1–6.
70. Ban, T., Hamada, D., Hasegawa, K., Naiki, H. & Goto, Y. (2003). Direct observation of amyloid fibril growth monitored by thioflavin T fluorescence. *J. Biol. Chem.* **278**, 16462–16465.
71. Schirra, R. (1985). Dye aggregation in freezing aqueous solutions. *Chem. Phys. Lett.* **119**, 463–466.
72. Retna Raj, R. R. C. (1997). γ-Cyclodextrin induced intermolecular excimer formation of thioflavin T. *Chem. Phys. Lett.* **273**, 285–290.
73. Groenning, M., Olsen, L., van de Weert, M., Flink, J. M., Frokjaer, S. & Jørgensen, F. S. (2007). Study on the binding of thioflavin T to β-sheet-rich and non-β-sheet cavities. *J. Struct. Biol.* **158**, 358–369.

74. Weiss, W. F., Hodgdon, T. K., Kaler, E. W., Lenhoff, A. M. & Roberts, C. J. (2007). Nonnative protein polymers: structure, morphology, and relation to nucleation and growth. *Biophys. J.* **93**, 4392–4403.
75. Gaczynska, M. & Osmulski, P. A. AFM of biological complexes: what can we learn? *Curr. Opin. Colloid Interface Sci.* In press. doi:10.1016/j.cocis.2008.01.004.
76. D'Alfonso, L., Collini, M. & Baldini, G. (2002). Does β-lactoglobulin denaturation occur via an intermediate state? *Biochemistry*, **41**, 326–333.
77. Strickler, S. J. & Berg, R. A. (1962). Relationship between absorption intensity and fluorescence lifetime of molecules. *J. Chem. Phys.* **37**, 814–822.
78. Miller, D. W. & Dill, K. A. (1997). Ligand binding to proteins: the binding landscape model. *Protein Sci.* **6**, 2166–2179.
79. Dobson, C. M. (1999). Protein misfolding, evolution and disease. *Trends Biochem. Sci.* **24**, 329–332.
80. Crick, S. L., Jayaraman, M., Frieden, C., Wetzel, R. & Pappu, R. V. (2006). Fluorescence correlation spectroscopy shows that monomeric polyglutamine molecules form collapsed structures in aqueous solutions. *Proc. Natl Acad. Sci. USA*, **103**, 16764–16769.
81. Vitalis, A., Wang, X. & Pappu, R. V. (2007). Quantitative characterization of intrinsic disorder in polyglutamine: insights from analysis based on polymer theories. *Biophys. J.* **93**, 1923–1937.
82. Messina, T. C., Kim, H., Giurleo, J. T. & Talaga, D. S. (2006). Hidden Markov model analysis of multichromophore photobleaching. *J. Phys. Chem. B*, **110**, 16366–16376.
83. Lawson, C. L. & Hanson, R. J. (1974). *Solving Least Squares Problems.* Prentice-Hall, Inc., Englewood Cliffs, NJ.
84. Provencher, S. W. (1982). A constrained regularization method for inverting data represented by linear algebraic or integral equations. *Comput. Phys. Commun.* **27**, 213–227.
85. Brown, W. (ed). (1993). Dynamic Light Scattering: The Method and Some Applications Oxford Science Publications, New York City, NY.